Deep hydrous mantle reservoir provides evidence for crustal recycling before 3.3 billion years ago

9 authors, including:

Alexander V Sobolev
Université Grenoble Alpes
250 PUBLICATIONS   **8,532** CITATIONS

SEE PROFILE

Evgeny Asafov
GEOKHI RAS
5 PUBLICATIONS   **68** CITATIONS

SEE PROFILE

Nicholas Arndt
University Joseph Fourier - Grenoble 1
335 PUBLICATIONS   **15,113** CITATIONS

SEE PROFILE

Gary Byerly
Louisiana State University
130 PUBLICATIONS   **3,871** CITATIONS

SEE PROFILE

Some of the authors of this publication are also working on these related projects:

Project Hotspot: The Snake River Plain Scientific Drilling Project View project

Heterogeneity of the Earth mantle View project

Deep hydrous mantle reservoir provides evidence for crustal recycling before 3.3 billion years ago

Alexander V. Sobolev[1,2], Evgeny V. Asafov[2], Andrey A. Gurenko[3], Nicholas T. Arndt[2], Valentina G. Batanova[1,2], Maxim V. Portnyagin[2,4], Dieter Garbe-Schönberg[5], Allan H. Wilson[6] and Gary R. Byerly[7]

[1] Université Grenoble Alpes, Institute Science de la Terre (ISTerre), CNRS, F-38041 Grenoble, France.

[2] Vernadsky Institute of Geochemistry and Analytical Chemistry, Russian Academy of Sciences, Kosygina str. 19, Moscow 119991, Russia.

[3] Centre de Recherches Pétrographiques et Géochimiques (CRPG), UMR 7358, Université de Lorraine, 54501 Vandœuvre-lès-Nancy, France.

[4] GEOMAR Helmholtz Centre for Ocean Research Kiel, Wischhofstrasse 1-3, 24148 Kiel, Germany.

[5] CAU Kiel University, Institute of Geosciences, Ludewig-Meyn-Strasse 10, 24118 Kiel, Germany.

[6] School of Geosciences, University of the Witwatersrand, Johannesburg 2050, South Africa

[7] Department of Geology and Geophysics, Louisiana State University, Baton Rouge, Louisiana 70803, USA.

First paragraph 262 words, main text 1868 words, 4 figures, 37 references.

H₂O strongly influences physical properties of the mantle and its ability to melt or convect and can trace recycling of surface reservoirs down to the deep mantle[1,2]. This makes knowledge of water content in the Earth's interior and its evolution through time crucial to understanding global geodynamics. Komatiites (MgO-rich ultramafic magmas) result from high-degree mantle melting at high pressures[3] and thus are excellent probes of H₂O contents in the deep mantle. A significant excess of H₂O over elements of similar geochemical behavior during mantle melting (e.g. Ce) was recently found in melt inclusions in the most Mg-rich olivine in 2.7 Ga old komatiites from Canada[4] and Zimbabwe[5]. These data were taken as evidence for a deep hydrated mantle reservoir, probably the transition zone, in the Neoarchean time. In this paper we confirm the mantle source of this H₂O by measurement of deuterium to hydrogen ratios in these melt inclusions and present similar data for 3.3 Ga old komatiites from the Barberton Greenstone Belt. Using hydrogen isotopes, we show that the mantle sources of these melts contained excess H₂O which implies that a deep mantle hydrated reservoir has been present in the Earth's interior at least since the Paleoarchean. The reconstructed initial hydrogen isotope composition of komatiites is significantly more depleted in deuterium than all surface reservoirs and typical mantle but resembles that in dehydrated subducted slabs. Together with a significant excess of chlorine and a temporal trend of Pb/Ce in the mantle sources of komatiites, these results argue that lithosphere recycling into the deep mantle, arguably via subduction, started before 3.3 Ga.

A common way to determine H₂O concentrations in the Earth's mantle is to measure them in submarine basaltic glasses (quenched and differentiated melts of mantle origin) or in glassy melt

45   inclusions in early crystallizing minerals of these lavas[1,2,6]. Because H_2O and Ce partition in a

46   similar way between minerals and melt, the H_2O/Ce ratio is independent of both fractionation and

47   degree of mantle melting and represents that of the mantle source. Most glasses from mantle

48   derived basalts at mid-ocean ridges and ocean islands show nearly constant H_2O/Ce = 200±100

49   implying a relatively narrow range of H_2O concentrations in the modern mantle (Fig. 1a). Magmas

50   originating over subduction zones gain H_2O through dehydration of the subducted slab and have

51   higher H_2O/Ce ratios (Fig 1a). The H_2O excess in these magmas positively correlates with the

52   excess of elements such as Ba and Rb that are concentrated in slab-derived hydrous fluids.

53

54   Melt inclusions in olivine from komatiites of different ages have Ba/Nb ratios similar to

55   Bulk Silicate Earth (BSE) but much higher H_2O/Ce ratios (Fig 1a). Our previous study of melt

56   inclusions in ca. 2.7 billion-year-old komatiites from the Abitibi[4] and Belingwe[5] greenstone belts

57   showed that their primary melts contained moderate water contents (0.2 to 0.6 wt% H_2O), but very

58   large excesses of H_2O over Ce. This feature was interpreted to indicate the presence of excessive

59   H_2O in their mantle sources, possibly entrained into the komatiite source as it passed through the

60   transition zone[4]. However, some melt inclusions in olivine also show an excess of H_2O over Ce

61   that was thought to originate from diffusive gain of H through the host olivine when the external

62   pressure of H_2O exceeded that inside the inclusion[7-9]. Such inclusions are identified in figure 1a.

63   However, the much more melt inclusions display significant H_2O depletion (H_2O/Ce ratios lower

64   than for syngeneic submarine glasses on Fig 1a) due to diffusive loss of H through the host olivine,

65   or by degassing of melt prior to entrapment[10,11].

66

67   Hydrogen isotopes are frequently used to trace the source of H_2O in mantle derived

68   magmas because of apparent disequilibria between deuterium enriched surface reservoirs and

69   deuterium depleted mantle[6]. They also efficiently record post-entrapment hydrogen exchange

70   between melt inclusions and external magma through host minerals as this process changes the

71   primordial H isotopic composition of melt inclusions because hydrogen (^1H) diffuses through

72   olivine much faster than deuterium (D) changing δD (the deviation in the ratio of $D/^1H$ in per mille

73   relative to the standard ratio in modern seawater, VSMOW) in melt inclusions[10-12] and also because

74   ^1H and D fractionate between melt and fluid[11]. The latter processes produce a negative correlation

75   between the δD and concentration of H_2O[10,11]. Despite these changes, hydrogen isotopes remain

76   sensitive tracers of the H_2O source - mantle, surface reservoirs or recycled material because their

77   fractionation between minerals and fluid at low and medium temperatures[6].

78

79   In this paper, we report the results of an investigation of melt inclusions in high-Mg olivine

80   phenocrysts in 3.3 billion-year-old komatiites from the Weltevreden Formation in the Barberton

81   greenstone belt (S. Africa)[13,14]. We used melt inclusions in olivine rather than bulk rock

82   compositions because these micro portions of melt were isolated by the host mineral and preserve

83   original contents of volatile and other highly mobile elements as shown before[4,5] and later in the

84   present study. We analyzed homogenized melt inclusions by electron microprobe for major and

85   minor elements, by laser ablation ICP-MS for trace elements and by ion probe for H_2O contents

86   (see METHODS). Hydrogen isotopes were analyzed by ion probe in selected melt inclusions (see

87   METHODS). Here we use these data to constrain the amount and origin of H_2O in the mantle

88   sources of these komatiites. Results are presented in Supplementary Tables 1-3.

89

90   H$_2$O/Ce ratios of melt inclusions display significant ranges for the same composition of the

91   host olivine (Fig 1b), a feature we attribute to H$_2$O loss or gain due to diffusion of H through

92   olivine or melt degassing prior to entrapment. The maximum H$_2$O/Ce ratio in each sample of

93   Weltevreden komatiites reversely correlates with the Fo content of host olivine. Because olivine

94   fractionation does not change the H$_2$O/Ce ratio, this suggests assimilation of H$_2$O-enriched

95   material during crystallization and emplacement of the Weltevreden komatiite.

96

97   Most measured hydrogen isotope compositions (δD) of melt inclusions in Weltevreden and

98   Abitibi komatiites show very high values that do not match any terrestrial reservoirs (Fig 2). In the

99   Weltevreden komatiite samples, δD increases with decreasing H$_2$O concentrations along tight

100   trajectories like those predicted for diffusional H loss[10]. Moreover, in samples 1521 and 1523, δD

101   correlates with the inclusion size (Extended data Fig 4). In Belingwe and sample 1521 from

102   Weltevreden komatiites, the δD values of the melt inclusions with the highest H$_2$O contents are

103   similar to that of Archean mantle (Fig 2). None of the measured δD values match the highly

104   negative numbers expected for melt inclusions that gained H by diffusion (Fig 2). These features

105   preclude diffusive gain of H$_2$O in the studied melt inclusions, and instead suggest partial diffusive

106   loss of H$_2$O from them. This result is in accord with that of our earlier study of melt inclusions in

107   olivines from Abitibi komatiites[4] in which we used Sc/Y olivine-melt geothermometry to estimate

108   the depression of crystallization temperatures caused by the presence of H$_2$O.

109

110   The original H isotope composition of the trapped melts was calculated using a model of

111   diffusional loss of hydrogen[10]. In our calculations, we used estimated initial H$_2$O contents of the

112   melt inclusions, their chemical compositions and size. The initial H$_2$O contents were inferred

113   assuming that the maximum H_2O/Al_2O_3 ratios in olivine-hosted melt inclusions in each sample

114   represents the minimum original amount of H_2O (see METHODS for further details). The

115   calculated mean isotopic compositions of hydrogen (Fig. 2) for Belingwe and Abitibi komatiites

116   and sample 1521 from Weltevreden are depleted in deuterium ($\delta D < -120‰$), and have

117   compositions that differ significantly from any surface H_2O reservoirs: in the latter, δD values are

118   thought to be close to 0 or slightly negative[6]. In contrast, the reconstructed δD values of melt

119   inclusions from samples 1523 and 1522 from Weltevreden are more enriched in deuterium and

120   their δD values are shifted towards those of hydrated rocks at the Earth's surface (sediments,

121   serpentinites), supporting their surface contamination proposed earlier based on evolution of

122   H_2O/Ce ratio (Fig 1b).

123

124   Our new data, as well as those reported earlier[4,5], rule out shallow contamination as a source

125   for H_2O excess in primitive komatiite melts from Abitibi, Belingwe and Weltevreden (except for

126   samples 1523 and 1522). Also, a primary source of the excess H_2O has been confirmed for

127   Gorgona komatiites[15]. None of these melts show the geochemical features of magmas from

128   subduction zones but are relatively enriched in chlorine (Fig 3). This suggests the persistence of a

129   deep hydrated mantle source from the Paleoarchean to at least the Tertiary (Fig 4a).

130

131   According to recent experimental data on the solidus temperature of fertile peridotite[16],

132   mantle plumes with potential temperatures over 1630°C, as is the case for the sources of Abitibi

133   and Belingwe komatiites[5], must have been partially molten in the mantle transition zone. The

134   composition of the primary melt for Weltevreden komatiites, calculated assuming equilibrium with

135   the most Mg-rich olivine (Fo 96, ref[13]), contains over 31 wt% MgO. This indicates an eruption

136   temperature of 1600°C (ca. 0.2 wt% H_2O) and a potential temperature over 1800°C [ref][17]. The

137   Weltevreden komatiites are more depleted in moderately incompatible elements than other

138   komatiites (Fig 3) and are thought to have originated by melting of a refractory source after the

139   extraction of partial melts in the plume, which also was partially molten in the mantle transitional

140   zone[18]. Ringwoodite and wadsleyite in the mantle transition zone have high storage capacities for

141   H_2O and Cl[19-21], and a significant amount of water appears to be present at these depths[22,23]. These

142   observations support an idea that water and possibly chlorine in these komatiites were entrained

143   into their plume sources during their passage through the hydrated transition zone[4]. The presence

144   of partial melt in the plume at the transition zone depths is thought to be essential for the

145   entrainment of volatiles[4]. The absence of H_2O excess in the magmas from classical Phanerozoic

146   mantle plumes like Hawaii or Iceland, which should also pass through the hydrated transition zone,

147   is attributed[4] to their lower temperature, which was not sufficiently high to produce partial melts

148   at transition zone depths.

149

150   The eruption temperature of Gorgona komatiite[24], calculated assuming an initial H_2O

151   content of 0.6 and 17 wt% MgO in the primary melt equilibrium with the most Fo-rich olivine

152   (Fo91.5) is only about 1360°C. On the other hand, the eruption temperatures of Gorgona picrites,

153   estimated from olivine compositions up to Fo93.6, and those of the picrites from Tortugal in

154   another part of the Caribbean large igneous province, are higher (up to 1570°C) and very close to

155   those of Archean komatiites[25,26]. This suggests that parts of the plume that produced the Gorgona

156   and Tortugal picrites were sufficiently hot that they were partially molten too when they passed

157   through the transition zone. In this case, the H_2O and chlorine reported in the Gorgona komatiites

158   could have been also derived from a hydrated reservoir in the transition zone.

159

160   The reconstruction of the original isotopic compositions of H in the trapped melts yields

161   an average δD less than -120‰. This is much more depleted in deuterium than any currently

162   accepted mantle composition (Fig 4b). Such a low δD could, however, correspond to that of a

163   lithospheric slab that was initially altered by seawater and then dehydrated during subduction[6,27].

164   This, and the excess of Cl, argue that the H_2O and Cl in the transition zone came from reacted

165   seawater that was transported into the deep mantle by partially dehydrated oceanic lithosphere.

166   Additional support of this hypothesis is the temporal trend of Pb/Ce in the mantle sources of

167   komatiites (Fig 4c). The canonical ratio Pb/Ce of mantle derived melts is a sensitive indicator of

168   the segregation of continental crust from the mantle[28,29]. Furthermore, because continental crust

169   production is a multistage process involving shallow recycling of materials processed at or close

170   to the Earth surface[28,29], the complement of this process in the deep mantle requires global

171   recycling of lithosphere down to the core-mantle boundary. As seen from Figure 4c, the deep

172   mantle sources of komatiites mimic the proposed global production of continental crust[30] with a

173   highly productive initial stage and a steady-state second stage. In addition, as shown recently[31],

174   the relatively low Si contents of 2.7 Ga old Abitibi komatiites suggest elevated carbon contents in

175   their mantle sources. Taken together, these results argue that subduction or other process able to

176   recycle surface materials down to deep mantle operated well before 3.3 Ga in accord with

177   consequences of recent geochemical and geodynamic modelling implying efficient crustal

178   recycling in Hadean and Archean eons[32].

179

180   The alternative explanation for the origin of deuterium-depleted mantle was recently

181   proposed based on the data on hydrogen isotope composition of melt inclusions in olivine from ca

182   60 million years old Baffin Island picrites[33]. These authors suggested the existence of primordial

183   reservoir with low deuterium to hydrogen ratio inherited from the protosolar nebula. However, the

184   reported melt inclusions do not show Cl and H_2O excesses typical for studied komatiites and thus

185   likely sampled a different reservoir.

186

196   **Author Information** All data used in this paper will be submitted to the Researchgate

197   (https://www.researchgate.net/profile/Alexander_Sobolev) and GEOROC (http://georoc.mpch-

198   mainz.gwdg.de/georoc/) databases. The authors declare no competing financial interests. Readers

199   are welcome to comment on the online version of the paper. Correspondence and requests for

200   materials should be addressed to A.V.S. (alexander.sobolev@ujf-grenoble.fr).

201

202   **Figures captions**

203

204   **Figure 1. Compositions of glasses and melt inclusions in olivine phenocrysts.**

205   **a.** H_2O/Ce and Ba/Nb ratios of melt inclusions in olivine in basalts (small grey dots), komatiites

206   (large filled circles) and glasses (coloured fields) from modern basalts (reference[34] and GEOROC

207   database: http://georoc.mpch-mainz.gwdg.de/georoc/) and from komatiites (references[4,5,15,24]

208   and this study).

209   Coloured fields correspond to submarine glasses of mid-ocean ridge basalts (MORB), ocean island

210   basalts (OIB), back arc basin basalts (BAB), island arc basalts (IAB), and continental margin basalts

211   and andesites (CMB). MORB and OIB form in mid-ocean ridges and intraplate settings while IAB

212   and CMB are directly related to subduction zones, BAB are barely related to subduction zones.

213   Primitive mantle composition after reference[35]. Specially marked by empty circle are melt

214   inclusions in olivine from basalts with gained H by diffusion through host olivine[8,9].

215   **b.** Compositions of melt inclusions versus Fo content of host olivine for komatiites. Variations of

216   H_2O/Ce ratios of inclusions in olivine of the same composition of host are attributed to post-

217   entrapment diffusional H loss. The increase of H_2O/Ce with decreasing Fo of host olivine in

218   Weltevreden samples is attributed to fractional crystallization plus wall-rock assimilation (AFC),

219   because olivine fractional crystallization (FC) alone does not change H_2O/Ce ratio of the melt. The

220   composition of hydrated transition zone (empty diamond) is estimated from H_2O contents of a

221   ringwoodite inclusion in diamond[22] and the Ce content of primitive mantle[35] assuming olivine

222   Fo90. The composition of mantle (pink field) is from[34,35]. Errors (2ste) are within symbol size.

223

224   **Figure 2. Measured and modelled H_2O contents and H isotope compositions of melt inclusions**

225   **in olivine from komatiites.**

226   Small symbols - measured compositions; Larger symbols - initial H_2O-δD (‰ VSMOW) in melt

227   inclusions reconstructed using the model of Buchloz et al,(2013) [10] (Methods) and measured

228   data. Error bars correspond to 2 standard errors. Reconstructed compositions for Weltevreden

229 komatiite samples 1522 and 1523 are marked by intermediate-sized symbols because they are

230 likely affected by contamination by surface materials. Dashed and dotted lines correspond to

231 trajectories due to diffusion H loss or gain through the host olivine[10]. Compositions of Archean

232 mantle and surface reservoirs are from reference [6].

233

234 **Figure 3. Primitive mantle normalized patterns of incompatible trace elements in trapped**

235 **melts in high-Mg olivine phenocrysts from komatiites.**

236 Compositions of melt inclusions in olivine Fo>91 from Gorgona komatiite (average of analyses by

237 reference[15]) and Archean komatiites studied in this paper (Extended data Table 1). Incompatible

238 element concentrations in the primitive mantle are from Hofmann et al, (1988)[35]; H_2O (266 ppm)

239 and Cl (26 ppm) are from Kentrick et al, (2015)[34].

240

241

242 **Figure 4. The temporal evolution of the komatiite mantle source composition and other Earth**

243 **reservoirs.**

244 **a.** Evolution of H_2O/Ce ratio in the mantle. The composition of hydrated transition zone is

245 estimated using the H_2O content of a ringwoodite inclusion in diamond[22], the Ce content of

246 primitive mantle[35] (large diamond; assigned an arbitrary age of 1.0 ± 0.5 Ga), and H_2O/Ce ratios

247 of melt inclusions in olivine (this paper and references[4,5,15]) and spinel[36] in komatiites. The

248 compositions of Phanerozoic mantle and bulk silicate earth (BSE) are from references[34,35].

249   **b**. Evolution of hydrogen isotope composition of mantle. Compositions of BSE, CRUST, MANTLE

250   and DEHYDRATED LITHOSPHERE and evolution of EARTH SURFACE AND EARTH MANTLE are from

251   reference[6].

252   **c**. Evolution of the Ce/Pb ratio in mantle sources of komatiites and the estimated production rate

253   of continental crust[30]. BSE composition after[35] and Phanerozoic mantle after[34]. Ce/Pb ratios of

254   melt inclusions of studied komatiites: Weltevreden 1521-26-9h, Abitibi 819-26-23, Belingwe Z6-

255   8-10; Lapland komatiite - calculated average of the least contaminated melt inclusions in spinel,

256   from Hanski and Kamenetsky (2013) [37].

257   All data plotted with 2 standard errors of mean (not seen if they are smaller than symbol size).

258   RDL-stands for Recycling of Dehydrated Lithosphere.

259

260   **REFERENCES**

261   1   Shaw, A. M. *et al.* Long-term preservation of slab signatures in the mantle inferred from
262   hydrogen isotopes. *Nature Geoscience* **5**, 224-228, doi:10.1038/ngeo1406 (2012).
263   2   Dixon, J. E. *et al.* Light Stable Isotopic Compositions of Enriched Mantle Sources:
264   Resolving the Dehydration Paradox. *Geochemistry Geophysics Geosystems* **18**, 3801-
265   3839, doi:10.1002/2016gc006743 (2017).
266   3   Herzberg, C. Depth and degree of melting of komatiites. *Journal of Geophysical*
267   *Research-Solid Earth* **97**, 4521-4540, doi:10.1029/91jb03066 (1992).
268   4   Sobolev, A. V. *et al.* Komatiites reveal a hydrous Archaean deep-mantle reservoir.
269   *Nature* **531**, 628-632, doi:10.1038/nature17152 (2016).
270   5   Asafov, E. V. *et al.* Belingwe komatiites (2.7 Ga) originate from a plume with moderate
271   water content, as inferred from inclusions in olivine. *Chemical Geology* **478**, 39-59,
272   doi:10.1016/j.chemgeo.2017.11.002 (2018).

273   6   Shaw, A. M., Hauri, E. H., Fischer, T. P., Hilton, D. R. & Kelley, K. A. Hydrogen isotopes in

274   Mariana arc melt inclusions: Implications for subduction dehydration and the deep-

275   Earth water cycle. *Earth and Planetary Science Letters* **275**, 138-145,

276   doi:10.1016/j.epsl.2008.08.015 (2008).

277   7   Portnyagin, M., Almeev, R., Matveev, S. & Holtz, F. Experimental evidence for rapid

278   water exchange between melt inclusions in olivine and host magma. *Earth and*

279   *Planetary Science Letters* **272**, 541-552, doi:10.1016/.j.epsl.2008.05.020 (2008).

280   8   Hartley, M. E., Neave, D. A., Maclennan, J., Edmonds, M. & Thordarson, T. Diffusive

281   over-hydration of olivine-hosted melt inclusions. *Earth and Planetary Science Letters*

282   **425**, 168-178, doi:10.1016/j.epsl.2015.06.008 (2015).

283   9   Jackson, M. G. *et al.* Ultra-depleted melts in olivine-hosted melt inclusions from the

284   Ontong Java Plateau. *Chemical Geology* **414**, 124-137,

285   doi:10.1016/j.chemgeo.2015.08.014 (2015).

286   10   Bucholz, C. E., Gaetani, G. A., Behn, M. D. & Shimizu, N. Post-entrapment modification of

287   volatiles and oxygen fugacity in olivine-hosted melt inclusions. *Earth and Planetary*

288   *Science Letters* **374**, 145-155, doi:10.1016/j.epsl.2013.05.033 (2013).

289   11   Hauri, E. SIMS analysis of volatiles in silicate glasses, 2: isotopes and abundances in

290   Hawaiian melt inclusions. *Chemical Geology* **183**, 115-141, doi:10.1016/s0009-

291   2541(01)00374-6 (2002).

292   12   Gaetani, G. A., O'Leary, J. A., Shimizu, N., Bucholz, C. E. & Newville, M. Rapid

293   reequilibration of H2O and oxygen fugacity in olivine-hosted melt inclusions. *Geology*

294   **40**, 915-918, doi:10.1130/g32992.1 (2012).

295   13   Connolly, B. D. *et al.* Highly siderophile element systematics of the 3.3 Ga Weltevreden

296   komatiites, South Africa: Implications for early Earth history. *Earth and Planetary*

297   *Science Letters* **311**, 253-263, doi:10.1016/j.epsl.2011.09.039 (2011).

298   14   Puchtel, I. S., Walker, R. J., Touboul, M., Nisbet, E. G. & Byerly, G. R. Insights into early

299   Earth from the Pt-Re-Os isotope and highly siderophile element abundance systematics

300   of Barberton komatiites. *Geochimica Et Cosmochimica Acta* **125**, 394-413,

301   doi:10.1016/j.gca.2013.10.013 (2014).

302 15 Gurenko, A. A., Kamenetsky, V. S. & Kerr, A. C. Oxygen isotopes and volatile contents of

303   the Gorgona komatiites, Colombia: A confirmation of the deep mantle origin of H2O.

304   *Earth and Planetary Science Letters* **454**, 154-165, doi:10.1016/j.epsl.2016.08.035

305   (2016).

306 16 Andrault, D. *et al.* Deep and persistent melt layer in the Archaean mantle. *Nature*

307   *Geoscience* **11**, 139-+, doi:10.1038/s41561-017-0053-9 (2018).

308 17 Herzberg, C. & Asimow, P. D. PRIMELT3 MEGA.XLSM software for primary magma

309   calculation: Peridotite primary magma MgO contents from the liquidus to the solidus.

310   *Geochemistry Geophysics Geosystems* **16**, 563-578, doi:10.1002/2014gc005631 (2015).

311 18 Robin-Popieul, C. C. M. *et al.* A New Model for Barberton Komatiites: Deep Critical

312   Melting with High Melt Retention. *Journal of Petrology* **53**, 2191-2229,

313   doi:10.1093/petrology/egs042 (2012).

314 19 Bercovici, D. & Karato, S. Whole-mantle convection and the transition-zone water filter.

315   *Nature* **425**, 39-44, doi:10.1038/nature01918 (2003).

316 20 Mibe, K., Orihashi, Y., Nakai, S. & Fujii, T. Element partitioning between transition-zone

317   minerals and ultramafic melt under hydrous conditions. *Geophysical Research Letters*

318   **33**, doi:10.1029/2006gl026999 (2006).

319 21 Roberge, M. *et al.* Is the transition zone a deep reservoir for fluorine? *Earth and*

320   *Planetary Science Letters* **429**, 25-32, doi:10.1016/j.epsl.2015.07.051 (2015).

321 22 Pearson, D. G. *et al.* Hydrous mantle transition zone indicated by ringwoodite included

322   within diamond. *Nature* **507**, 221-+, doi:10.1038/nature13080 (2014).

323 23 Tschauner, O. *et al.* Ice-VII inclusions in diamonds: Evidence for aqueous fluid in Earth's

324   deep mantle. *Science* **359**, 1136-+, doi:10.1126/science.aao3030 (2018).

325 24 Kamenetsky, V. S., Gurenko, A. A. & Kerr, A. C. Composition and temperature of

326   komatiite melts from Gorgona Island, Colombia, constrained from olivine-hosted melt

327   inclusions. *Geology* **38**, 1003-1006, doi:10.1130/g31143.1 (2010).

328 25 Revillon, S., Arndt, N. T., Chauvel, C. & Hallot, E. Geochemical study of ultramafic

329   volcanic and plutonic rocks from Gorgona Island, Colombia: The plumbing system of an

330   oceanic plateau. *Journal of Petrology* **41**, 1127-1153, doi:10.1093/petrology/41.7.1127

331   (2000).

332 26 Trela, J. *et al.* The hottest lavas of the Phanerozoic and the survival of deep Archaean

333   reservoirs. *Nature Geoscience* **10**, 451-+, doi:10.1038/ngeo2954 (2017).

334 27 Walowski, K. J., Wallace, P. J., Hauri, E. H., Wada, I. & Clynne, M. A. Slab melting beneath

335   the Cascade Arc driven by dehydration of altered oceanic peridotite. *Nature Geoscience*

336   **8**, 404-+, doi:10.1038/ngeo2417 (2015).

337 28 Chauvel, C., Goldstein, S. L. & Hofmann, A. W. Hydration and dehydration of oceanic-

338   crust controls Pb evolution in the mantle. *Chemical Geology* **126**, 65-75,

339   doi:10.1016/0009-2541(95)00103-3 (1995).

340 29 Hofmann, A. W. Mantle geochemistry: The message from oceanic volcanism. *Nature*

341   **385**, 219-229, doi:10.1038/385219a0 (1997).

342 30 Dhuime, B., Hawkesworth, C. J., Cawood, P. A. & Storey, C. D. A Change in the

343   Geodynamics of Continental Growth 3 Billion Years Ago. *Science* **335**, 1334-1336,

344   doi:10.1126/science.1216066 (2012).

345 31 Herzberg, C. Petrological Evidence from Komatiites for an Early Earth Carbon and Water

346   Cycle. *Journal of Petrology* **57**, 2271-2287, doi:10.1093/petrology/egw055 (2016).

347 32 Rosas, J. C. & Korenaga, J. Rapid crustal growth and efficient crustal recycling in the early

348   Earth: Implications for Hadean and Archean geodynamics. *Earth and Planetary Science*

349   *Letters* **494**, 42-49, doi:10.1016/j.epsl.2018.04.051 (2018).

350 33 Hallis, L. J. *et al.* Evidence for primordial water in Earth's deep mantle. *Science* **350**, 795-

351   797, doi:10.1126/science.aac4834 (2015).

352 34 Kendrick, M. A. *et al.* Seawater cycled throughout Earth's mantle in partially

353   serpentinized lithosphere. *Nature Geoscience* **10**, 222-U297, doi:10.1038/ngeo2902

354   (2017).

355 35 Hofmann, A. W. Chemical differentiation of the Earth: the relationship between mantle,

356   continental crust, and oceanic crust. *Earth Planet. Sci. Lett.* **90**, 297-314 (1988).

357 36 Shimizu, K., Komiya, T., Hirose, K., Shimizu, N. & Maruyama, S. Cr-spinel, an excellent

358   micro-container for retaining primitive melts - implications for a hydrous plume origin

359   for komatiites. *Earth and Planetary Science Letters* **189**, 177-188, doi:10.1016/s0012-

360   821x(01)00359-4 (2001).

361   37   Hanski, E. & Kamenetsky, V. S. Chrome spinel-hosted melt inclusions in Paleoproterozoic

362   primitive volcanic rocks, northern Finland: Evidence for coexistence and mixing of

363   komatiitic and picritic magmas. *Chemical Geology* **343**, 25-37,

364   doi:10.1016/j.chemgeo.2013.02.009 (2013).

365

METHODS (1764 words)

Samples

<u>Weltevreden Formation komatiites.</u> We selected three samples of 3.3 Ga Weltevreden komatiites for this study that came from the well-preserved parts of the cumulate zones of three separate flows (Extended Data Figure 1) of Saw Mill area of the Weltevreden Formation of Barberton Greenstone Belt, South Africa[38]. These are the massive komatiite cumulates consisting of partially unaltered olivine, spinel and clinopyroxene grains of different size and composition. Details of the samples are as follows:

Sample 1521 (Gary's flow #2) is an olivine cumulate that contains large (up to 2 mm in diameter) partially serpentinized euhedral olivine grains with high-Fo contents (93.5–95.5 mol% Fo). The interstitial groundmass of the rock is made of acicular clinopyroxene (up to 1 mm in diameter), equant or skeletal spinel (up to 100 μm in diameter, Cr-number up to 81 [$Cr/(Cr+Fe^{3+}+Ti+Al)$] and the altered volcanic glass. Sample 1522 (Keena's flow #1) is an olivine cumulate made of partially serpentinized euhedral olivine grains (1.5 mm in diameter, with a range of olivine compositions – 93.7-95.1 mol% Fo), acicular (up to 0.5 mm in diameter) clinopyroxene, skeletal and to lesser extent equant spinel grains (up to 100μm) and interstitial completely altered volcanic

382 glass. Sample 1523 (Keena's flow #2) – olivine cumulate consisting of partially serpentinized

383 euhedral olivine grains of different size (mainly 1-1.5 mm, with individual grains up to 2.5 mm in

384 diameter; 93-93.9 mol% Fo). The interstitial groundmass is made of acicular clinopyroxene (up to

385 1 mm in diameter), equant and skeletal spinel crystals (up to 100 µm in diameter, Cr-number 77-

386 82) and completely altered volcanic glass.

387 Abundant partially crystallized melt inclusions (few-200 µm in diameter) composed of glass,

388 olivine, clinopyroxene and spinel occur in the olivine grains (Extended Data Figure 2a).

389 Abitibi and Belingwe Greenstone Belts. Studied samples M810 (Pike Hill) and Z6 (Zimbabwe)

390 are described in references [4] and [5] correspondingly.

391 **Analytical methods**

392 To study the compositions of minerals and glasses we used the following in situ analytical

393 techniques: electron probe microanalysis (EPMA), secondary ion mass-spectrometry (SIMS) and

394 laser-ablation ICP-MS.

395 EPMA. Melt inclusions, host olivine and spinel were analysed for major and minor elements on

396 a JEOL JXA 8230 microprobe at ISTerre in Grenoble, France using methods and protocols

397 described in ref. [4].

398 SIMS. Hydrogen abundance and D/H ratios of olivine-hosted melt inclusions were analysed by

399 the CAMECA IMS 1280 HR2 ion microprobe at the *Centre de Recherches Pétrographiques et*

400 *Géochimiques* (CRPG, Nancy, France). The inclusion-bearing olivine grains recovered from the

401 laboratory heating experiments, mounted in epoxy resin beds and analysed for major elements by

402 EPMA, were carefully re-polished to remove carbon coating, using consequently 1-µm-grain-size

403 Al_2O_3 and 0.25-µm-grain-size SiO_2 suspensions. The grains were then removed from the epoxy,

404 remounted by pressing them into two indium metal mounts, which were ultrasonically cleaned and

405 stored in a laboratory heating and drying oven at about +70 °C for 24 hours. Immediately after

406 gold coating and about 24 to 48 hours prior to analysis, the mounts were placed into a sample

407 storage of the ion probe and held at a pressure of ~10^{-8} Torr to lower H_2O blank.

408

409 The samples were sputtered with a 10-kV, 1.5–3.2-nA, $^{133}Cs^+$ primary beam focused to a spot of

410 5–10 μm, rastered to 20 μm × 20 μm during 180 s pre-sputtering (in order to further clean the

411 sample surface), and to 10 μm × 10 μm during analysis. A normal-incidence electron gun used for

412 sample charge compensation was tuned by limiting the H^- emission from the sample surface to

413 <1000 cps. A mechanical field aperture of ~1,000 μm was set at the secondary ion image plane

414 in order to eliminate the secondary ion signal from the spot margins. A liquid-nitrogen cold trap

415 and a sublimation pump were used to maintain a sample chamber pressure of ≤10^{-10} Torr during

416 analyses. An energy slit was centred and opened to 30 eV.

417

418 After pre-sputtering, the intensities of $^{17}O^-$ (counting time 2 s), $^{16}OH^-$ (6 s), $^{18}O^-$ (4 s), $^{17}OH^-$ (4 s)

419 and $^{16}OD^-$ (20 s) secondary ions were measured in monocollection mode during 30 to 60 cycles

420 (depending on the H_2O concentration in the analysed glasses), using axial electron multiplier

421 (EM). The EM dead time correction (45 ns measured during the analytical session) was applied to

422 all masses. A mass-resolving power ($M/\Delta M$) of ~13,000, suicient to resolve ^{16}OD mass from $^{16}OH_2$

423 ($M/\Delta M$ = 11,632) and ^{17}OH ($M/\Delta M$ = 8,739) interferences, was applied.

424

425   The analyses were performed during one 7-day-long analytical session from 29 January through

426   4 February, 2018. To establish calibration curves between measured $^{16}OH^-/^{18}O^-$ the respective

427   H_2O concentrations, a set of 7 natural and synthetic reference glasses of basaltic composition

428   (Extended fig. 3a, Supplementary Table 4ab) were analysed at the beginning and throughout the

429   analytical session, with at least 3 to 7 replicate measurements. In addition, a synthetic forsterite

430   (4.5 ± 1 µg/g H_2O) and a synthetic Suprasil 3002 quartz glass (0.99 ± 0.36 µg/g H_2O)[39] were

431   repeatedly analysed during the analytical session to monitor the $^{16}OH^-$ background level. Under

432   these analytical conditions, typical count rates were ~7.6 × 10^{+5} cps for $^{16}OH^-$ and ~152 cps for

433    $^{16}OD^-$ on ETNA-0 (1.35 wt.% H_2O) and ~1.1 × 10^{+5} cps for $^{16}OH^-$ and ~23 cps for $^{16}OD^-$ on CL-DR01-

434   5V (0.17 wt.% H_2O) reference glasses. For comparison, ~3.3 × 10^{+2} cps for $^{16}OH^-$ and ~0.54 cps

435   for $^{16}OD^-$ were measured on the Suprasil 3002 quartz glass and ~4.8 × 10^{+2} cps for $^{16}OH^-$ and

436   ~0.57 cps for $^{16}OD^-$ on the synthetic olivine. The calibration curve for H_2O yields a relative error

437   of ±5.1% (Extended Data Figure 3a).

438

439   The hydrogen isotopic compositions are reported as δD values calculated as:

440

441   δD (‰) = [(D/H)$_{sample}$ / (D/H)$_{VSMOW}$−1] × 1000, (1)

442   where (D/H)$_{VSMOW}$ = 155.76 × 10^{-6}

443

444   The measured δD values (δD_{meas}) are biased by instrumental mass fractionation of H and D

445   isotopes (*IMF*, ‰, see details in Supplementary Table 4), which depends on matrix composition[40].

446   To determine matrix effect for our measurements we applied a multivariate linear correlation (*p*-

447   *value* <0.002, R^2 ~0.75) between the *IMF* values and the concentrations of Al_2O_3 and H_2O in the

448   5 glass standards (60701, 40428, CY82-29-3V, VG-2 USNM111240 and ETNA-0, Extended Data

449   Figure 3b,c):

450

451        $IMF = 439.74711 - 20.34088 \times H_2O + 4.76916 \times Al_2O_3$ (2)

452

453   Using the equation (2), the matrix effect on the *IMF* was ceased and the δD_{true} values were

454   calculated as

455

456        $\delta D_{meas} - IMF = \delta D_{true}$ (3)

457

458   The reported error, calculated as average residuals for the obtained regression, is ±6.3‰.

459   **Laser-ablation ICP-MS**

460   Trace-element concentrations in melt inclusions and host olivine were analysed by laser ablation

461   ICP-MS using an Agilent 7900 quadrupole mass-spectrometer coupled with a 193 nm Excimer

462   Laser Ablation system GeoLas Pro (Coherent) at the Institute of Geosciences of Kiel University,

463   Germany. Analyses were performed with 24-μm and 60 to 90-μm spots for inclusions and olivine,

464   respectively, 10 Hz pulse frequency, and a laser fluence of 5 J cm^{-2}. In total, 41 elements were

465   measured. Dwell times ranged from 2 ms for major elements to 20 ms for the least abundant trace

466   elements (e.g., Pb, Th, HREE) with total time per cycle of 0.61 s. The other instrumental conditions

467   and data reduction scheme were the same as in reference [4].

Melt inclusions

Olivine fractions were placed into the platinum capsules and heated at 1 atm pressure in the CO_2-H_2 gas mixture corresponding to QFM-1 oxygen fugacity in a vertical furnace at Vernadsky Institute in Moscow, Russia[41] in order to homogenize the partially crystallized melt inclusions. Samples were heated to 800°C for 5 min to exhaust the atmosphere gas then the experimental temperature was raised to 1450-1520°C for 5 min. Olivine grains were then quenched, mounted in epoxy and polished to expose the glassy melt inclusions on the surface. Though the melt inclusions contain a shrinkage bubble (Extended Data Figure 2b-d) some of them were completely homogenized (Extended Data Figure 2e,f). The melt inclusions that were analysed were larger than 20 μm in diameter because smaller inclusions commonly demonstrate bias in their chemical compositions due to the boundary layer effects. Melt inclusions that had been altered and cracked before or during the experiment were identified by the low S concentrations (below 100 ppm) and were excluded.

The composition of the glasses of melt inclusions are commonly modified by the Fe-Mg diffusional exchange with the olivine hosts and by the olivine crystallization on the walls of the melt inclusions[42]. Thus, the measured compositions were corrected using the reverse Fe-Mg exchange[43,44] and applying the olivine-melt equilibrium model[45] and the estimated FeO contents of the trapped melts. For the Weltevreden samples the FeO contents of the included melts were estimated as a function of Fo contents of equilibrium olivine through modeling the crystallization of random spinifex komatiite KBA 12-10 [46], which is suggested to represent the initial magma composition. The original trapped melt compositions of the Belingwe and Abitibi komatiites were reconstructed as described in [4] and [5].

490   **Hydrogen isotope modelling.**

491   Hydrogen isotope compositions of melt inclusions indicate H loss from inclusions to external

492   system by volume diffusion through host olivine (Figure 2; Extended data Figure 4). In order to

493   reverse this process and estimate the initial isotope composition of hydrogen the initial content of

494   H_2O in melt inclusions is required to be known. These concentrations were inferred assuming that

495   the maximum H_2O/Al_2O_3 ratios in olivine-hosted melt inclusions in each sample represent the

496   minimum original amount of H_2O. We use the Al_2O_3 content of the trapped melt inclusions as a

497   reference because being incompatible with olivine it mimics perfectly the olivine crystallization

498   trend (Extended Data Figure 5a). Thus, the ratio of H_2O (other component incompatible with

499   olivine) to Al_2O_3 has to be constant during olivine crystallization and could decrease due to H loss

500   from inclusion. Corrected for H loss initial H_2O contents of trapped melt inclusions of the

501   Weltevreden komatiites also yield olivine control trends for each sample but show significant

502   difference between samples (Extended Data Figure 5b).

503   The original H isotope composition of the trapped melts was calculated using a model of

504   diffusional loss of hydrogen[14]. In our calculations, we used estimated initial H_2O contents of the

505   melt inclusions, their chemical compositions and sizes. The external pressure and H_2O content

506   were assumed to be 1 bar and 0%, the size of olivine crystals was taken as 1 mm, and the

507   temperature as 1400°C, oxygen fugacity QFM-1.

508   Hydration of melt inclusions by diffusional gain of H was modelled using the same protocol[14], but

509   assuming external pressure and H_2O contents of 100 bars and 0.5 wt% respectively, inclusion size

22

510   of 50 μm in diameter, composition of melt inclusion as 1521-26-9h and different initial water

511   concentrations of melt inclusions.

512

513   REFERENCES

38   Byerly, B. L., Kareem, K., Bao, H. M. & Byerly, G. R. Early Earth mantle heterogeneity revealed by

        light oxygen isotopes of Archaean komatiites. *Nature Geoscience* **10**, 871-+,

        doi:10.1038/ngeo3054 (2017).

39   Wetzel, D. T., Hauri, E. H., Saal, A. E. & Rutherford, M. J. Carbon content and degassing history

        of the lunar volcanic glasses. *Nature Geoscience* **8**, 755-758 (2015).

40   Hauri, E. H. *et al.* Matrix effects in hydrogen isotope analysis of silicate glasses by SIMS.

        Chemical Geology **235**, 352-365, doi:10.1016/j.chemgeo.2006.08.010 (2006).

41   Krasheninnikov, S. P., Sobolev, A. V., Batanova, V. G., Kargaltsev, A. A. & Borisov, A. A.

        Experimental testing of olivine-melt equilibrium models at high temperatures. *Doklady Earth

        Sciences* **475**, 919-922, doi:10.1134/s1028334x17080153 (2017).

42   Sobolev, A. V. & Danyushevsky, L. V. Petrology and geochemistry of boninites from the North

        termination of the Tonga trench - constraints on the generation conditions of primary high-ca

        boninite magmas. *Journal of Petrology* **35**, 1183-1211 (1994).

43   Danyushevsky, L. V., Della-Pasqua, F. N. & Sokolov, S. Re-equilibration of melt inclusions

        trapped by magnesian olivine phenocrysts from subduction-related magmas: petrological

        implications. *Contributions to Mineralogy and Petrology* **138**, 68-83, doi:10.1007/pl00007664

        (2000).

44   Danyushevsky, L. V. & Plechov, P. Petrolog3: Integrated software for modeling crystallization

processes. *Geochemistry Geophysics Geosystems* **12**, doi:10.1029/2011gc003516 (2011).

45   Ford, C. E., Russell, D. G., Craven, J. A. & Fisk, M. R. Olivine liquid equilibria - temperature,

pressure and composition dependence of the crystal liquid cation partition-coefficients for Mg,

Fe-2+, Ca and Mn. *Journal of Petrology* **24**, 256-265 (1983).

46   Kareem, K. *Komatiites of the Weltevreden Formation, Barberton Greenstone Belt, South Africa:*

implications for the chemistry and temperature of the Archean mantle. Doctor of Philosophy

thesis, Baton Rouge, Louisiana State University, (2005).

47   Asafov E.V., Sobolev A.V., Gurenko A.A., Arndt N.T., Batanova V.G., Portnyagin M.V., Garbe-

Schönberg D., Krasheninnikov S.P., A. H. Wilson and G.R. Byerly, Olivine-Hosted Melt Inclusions

in the Ancient Komatiites – the Potential Key to the Archean Mantle Composition//Abstracts,

S3.T02, p.50, ECROFI-2017
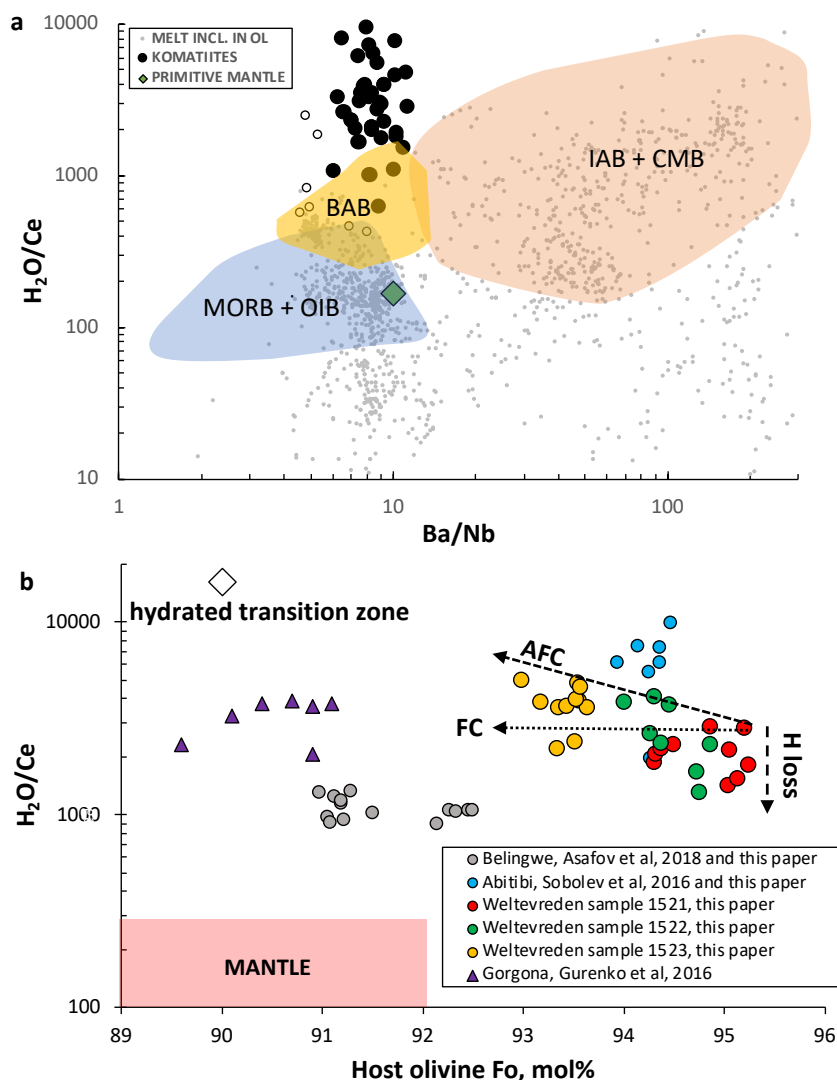
Figure 1. *Compositions of glasses and melt inclusions in olivine phenocrysts.*

a. H_2O/Ce and Ba/Nb ratios of melt inclusions in olivine in basalts (small grey dots), komatiites (large filled circles) and glasses (coloured fields) from modern basalts (reference[34] and GEOROC database: http://georoc.mpch-mainz.gwdg.de/georoc/) and from komatiites (references[4,5,15,24] and this study).
Coloured fields correspond to submarine glasses of mid-ocean ridge basalts (MORB), ocean island basalts (OIB), back arc basin basalts (BAB), island arc basalts (IAB), and continental margin basalts and andesites (CMB). MORB and OIB form in mid-ocean ridges and intraplate settings while IAB and CMB are directly related to subduction zones, BAB are barely related to subduction zones. Primitive mantle composition after reference[35]. Specially marked by empty circle are melt inclusions in olivine from basalts with gained H by diffusion through host olivine[8,9].

b. Compositions of melt inclusions versus Fo content of host olivine for komatiites. Variations of H_2O/Ce ratios of inclusions in olivine of the same composition of host are attributed to post-entrapment diffusional H loss. The increase of H_2O/Ce with decreasing Fo of host olivine in Weltevreden samples is attributed to fractional crystallization plus wall-rock assimilation (AFC), because olivine fractional crystallization (FC) alone does not change H_2O/Ce ratio of the melt. The composition of hydrated transition zone (empty diamond) is estimated from H_2O contents of a ringwoodite inclusion in diamond[22] and the Ce content of primitive mantle[35] assuming olivine Fo90. The composition of mantle (pink field) is from[34,35]. Errors (2ste) are within symbol size.
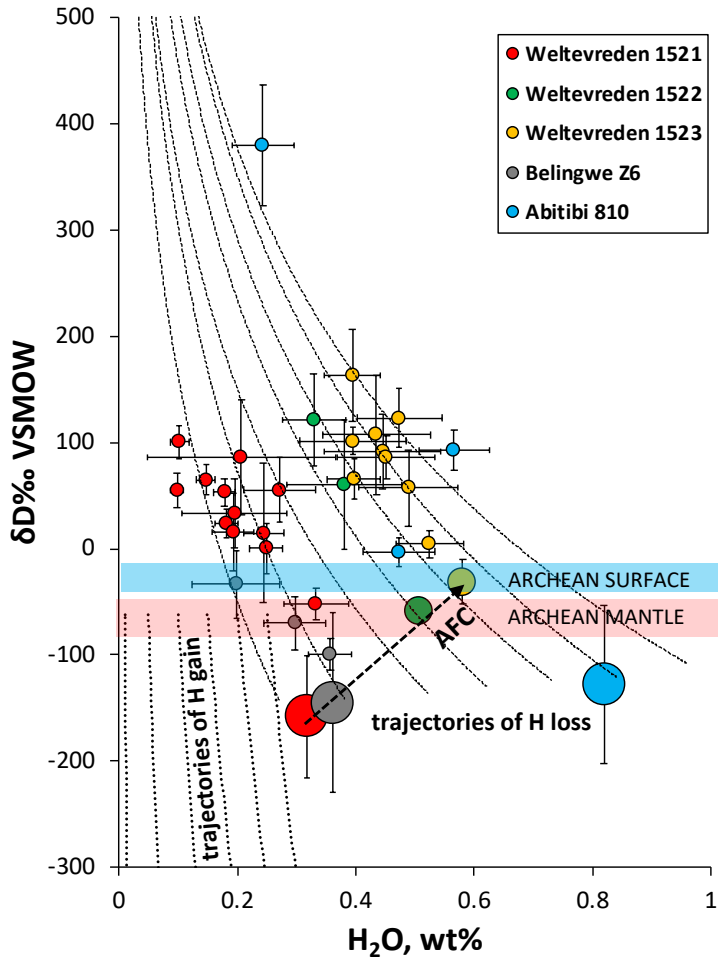
Figure 2. Measured and modelled H₂O contents and H isotope compositions of melt inclusions in olivine from komatiites.

Small symbols - *measured compositions;* Larger symbols - *initial H₂O-δD (‰ VSMOW) in melt inclusions reconstructed using the model of Buchloz et al,(2013) [10] (Methods) and measured data. Error bars correspond to 2 standard errors. Reconstructed compositions for Weltevreden komatiite samples 1522 and 1523 are marked by intermediate-sized symbols because they are likely affected by contamination by surface materials. Dashed and dotted lines correspond to trajectories due to diffusion H loss or gain through the host olivine[10]. Compositions of Archean mantle and surface reservoirs are from reference [6].*
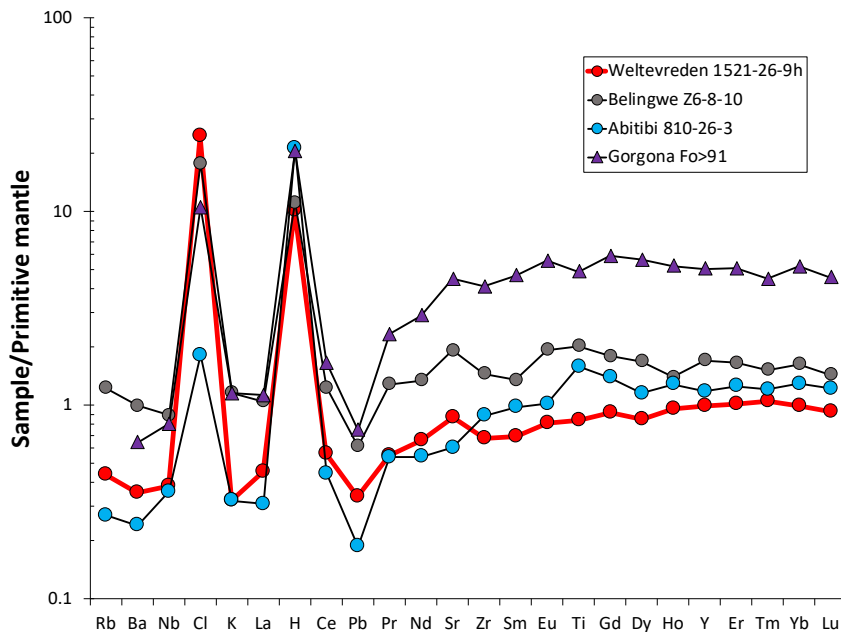
Figure 3. Primitive mantle normalized patterns of incompatible trace elements in trapped melts in high-Mg olivine phenocrysts from komatiites.

Compositions of melt inclusions in olivine Fo>91 from Gorgona komatiite (average of analyses by reference[15]) and Archean komatiites studied in this paper (Extended data Table 1). Incompatible element concentrations in the primitive mantle are from Hofmann et al, (1988)[35]; H₂O (266 ppm) and Cl (26 ppm) are from Kentrick et al, (2015)[34].
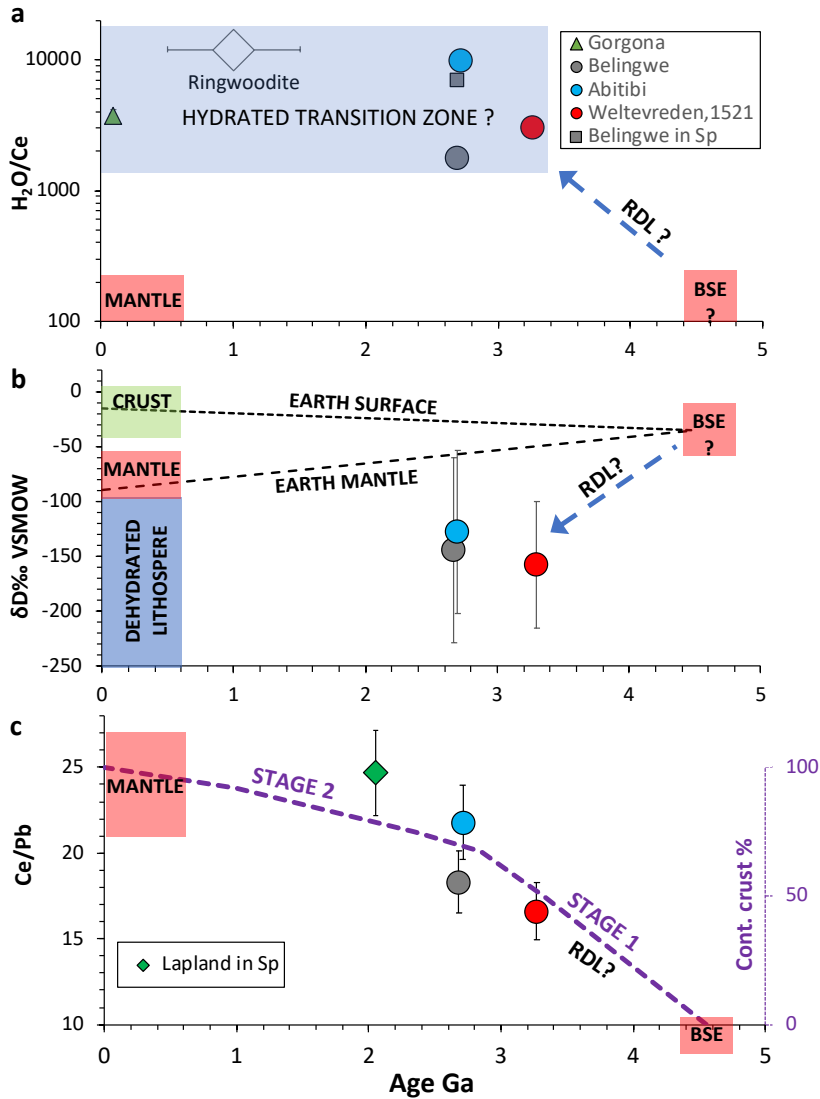
Figure 4. *The temporal evolution of the komatiite mantle source composition and other Earth reservoirs*.

a. Evolution of H_2O/Ce ratio in the mantle. The composition of hydrated transition zone is estimated using the H_2O content of a ringwoodite inclusion in diamond[22], the Ce content of primitive mantle[35] (large diamond; assigned an arbitrary age of 1.0 ± 0.5 Ga), and H_2O/Ce ratios of melt inclusions in olivine (this paper and references[4,5,15]) and spinel[36] in komatiites. The compositions of Phanerozoic mantle and bulk silicate earth (BSE) are from references[34,35].

b. Evolution of hydrogen isotope composition of mantle. Compositions of BSE, CRUST, MANTLE and DEHYDRATED LITHOSPHERE and evolution of EARTH SURFACE AND EARTH MANTLE are from reference[6].

c. Evolution of the Ce/Pb ratio in mantle sources of komatiites and the estimated production rate of continental crust[30]. BSE composition after[35] and Phanerozoic mantle after[34]. Ce/Pb ratios of melt inclusions of studied komatiites: Weltevreden 1521-26-9h, Abitibi 819-26-23, Belingwe Z6-8-10; Lapland komatiite - calculated average of the least contaminated melt inclusions in spinel, from Hanski and Kamenetsky (2013) [37].

All data plotted with 2 standard errors of mean (not seen if they are smaller than symbol size). RDL-stands for Recycling of Dehydrated Lithosphere.
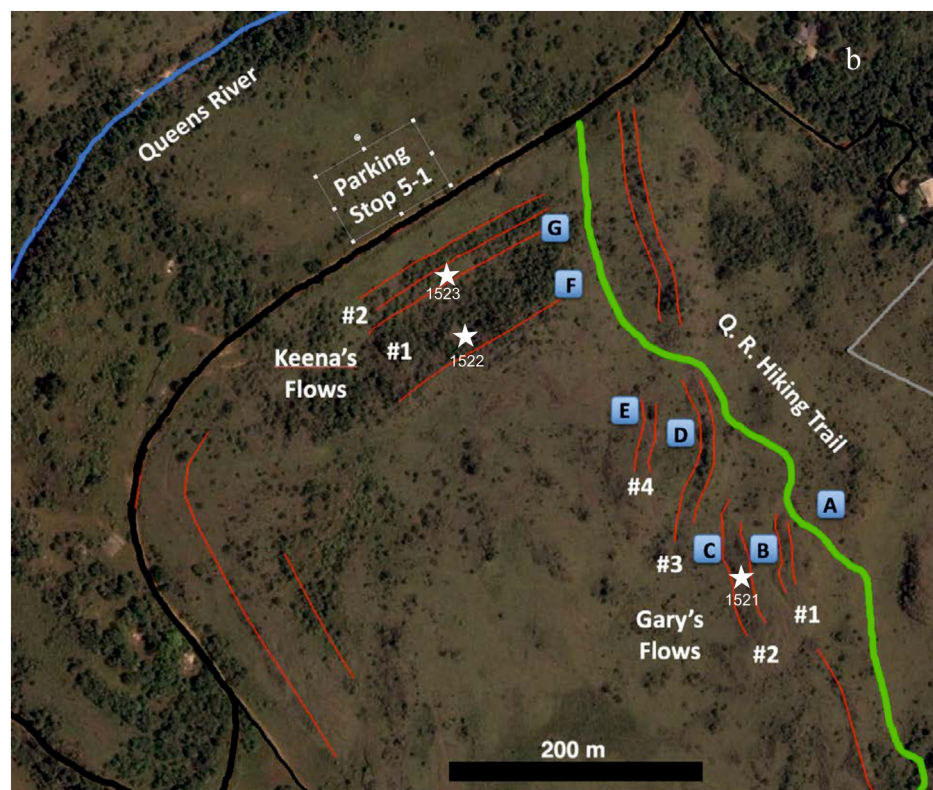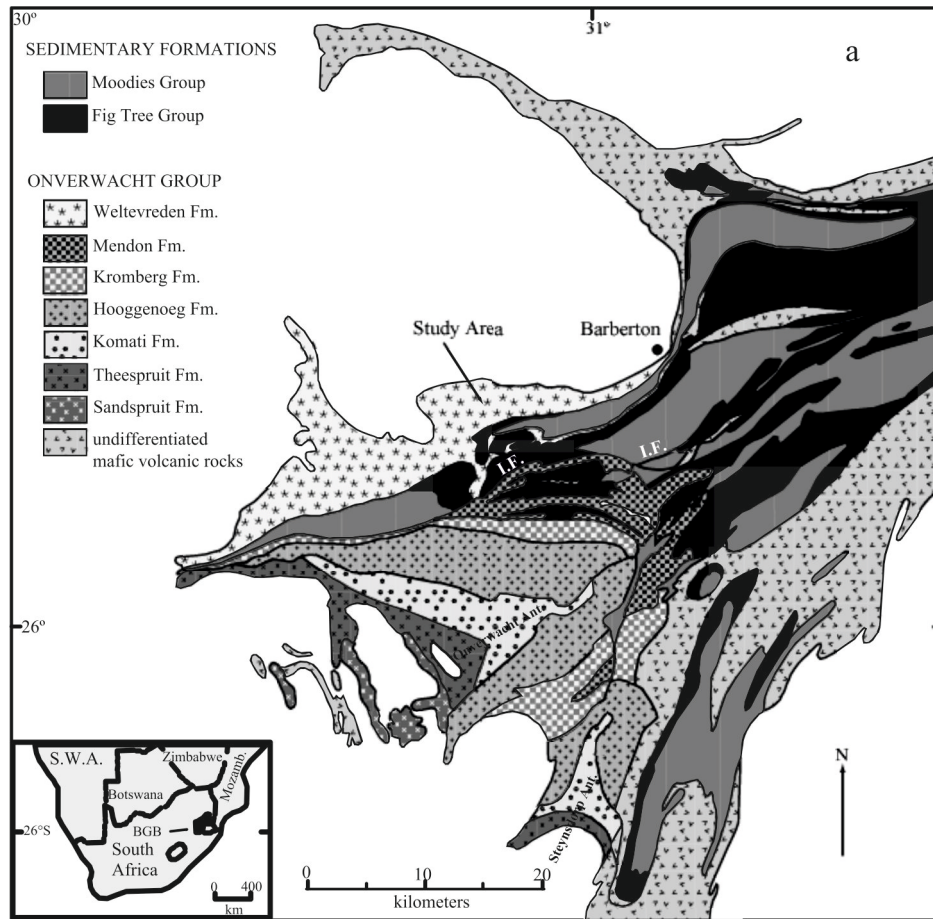
Extended Data Figure 1 |a. Generalized geologic map of the western half of the Barberton Greenstone Belt (modified after[46]). **b**. Field locality of the sampling area (Saw Mill area, Weltevreden formation, modified after[38]).
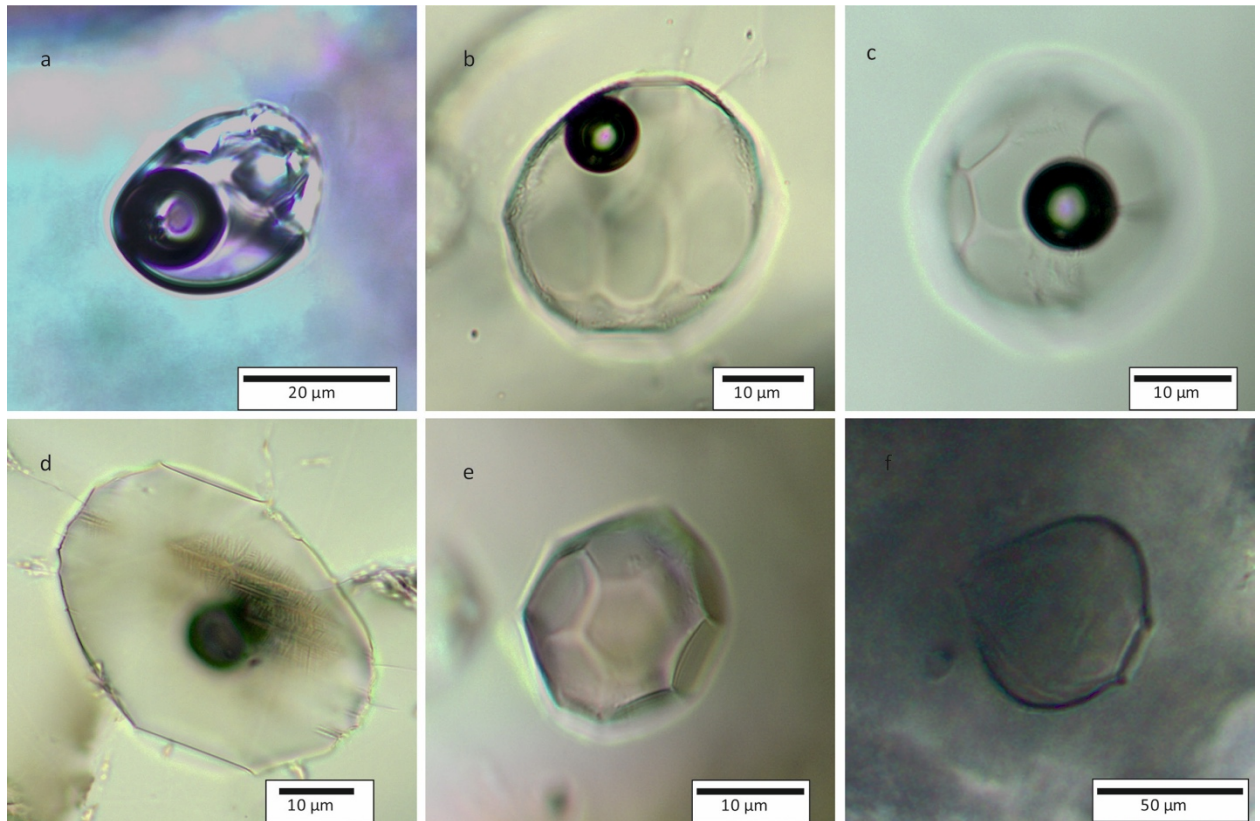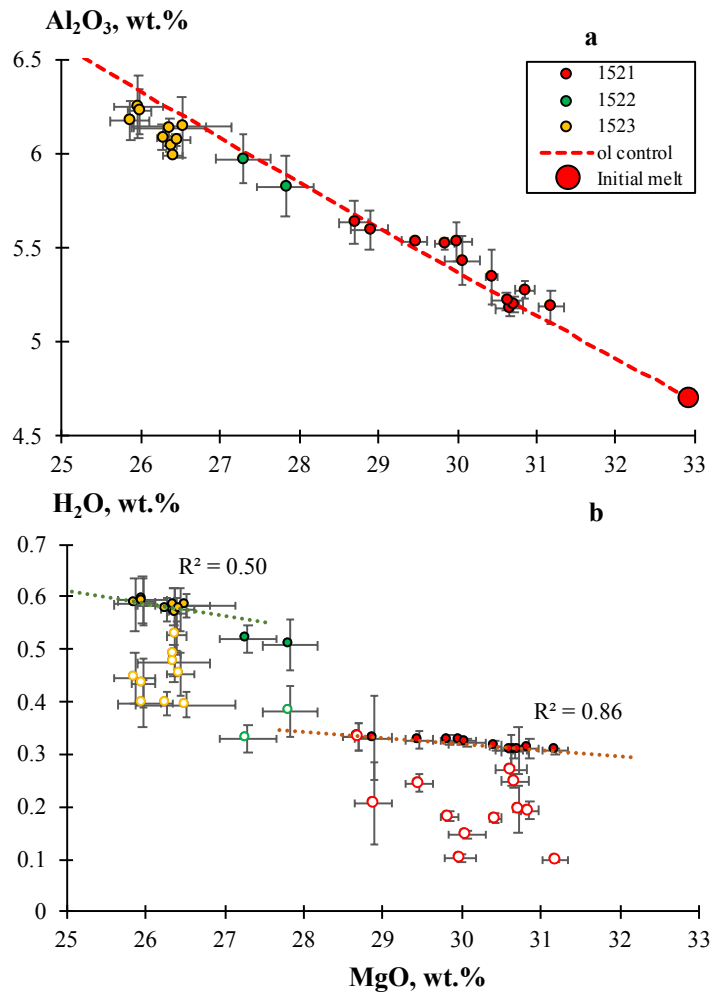
Extended Data Figure 2 |Olivine hosted melt inclusions (sample 1521) from the 3.3 Ga Weltevreden komatiites: **a** - untreated partially crystallized melt inclusion containing clinopyroxene, glass and the shrinkage bubble; **b, c, d, e** and **f** – glassy melt inclusions after the quenching experiments (see METHODS); **b,c** and **d** – contain shrinkage bubble; **d** – contains fine olivine spinifex textures due to very high MgO contents of the melt (>26 wt.% MgO); **e** and **f** – homogeneous melt inclusions, **f**- the 1521-9h melt inclusion reported in this study.
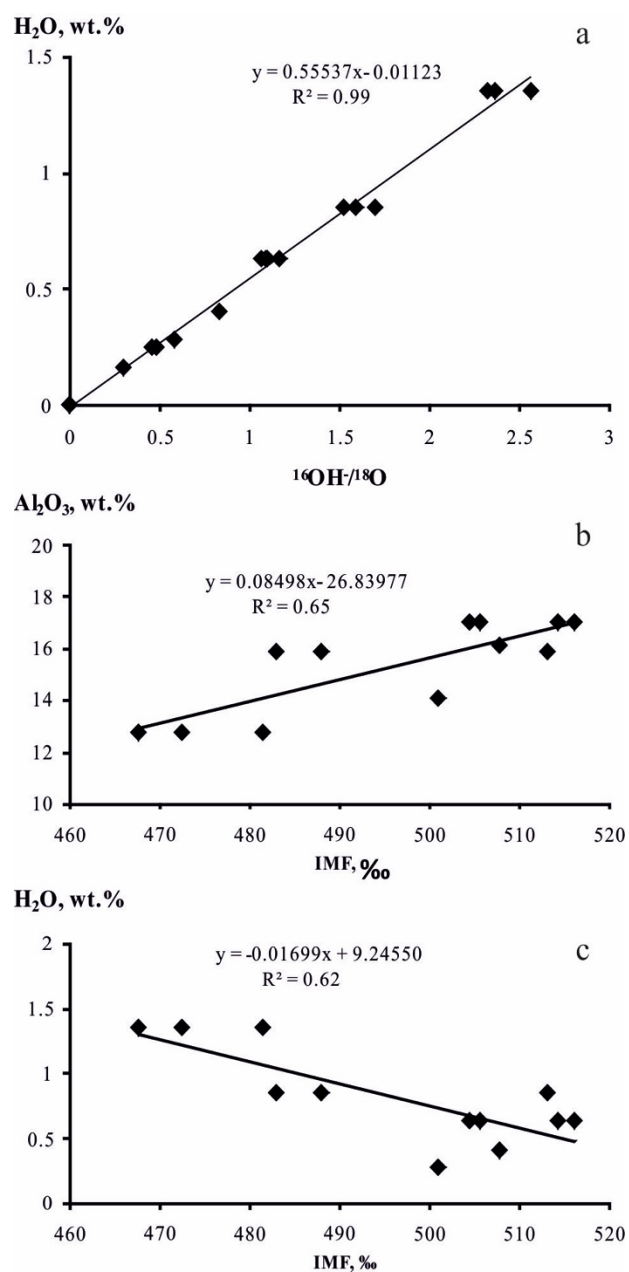
Extended Data Figure 3 | a – H_2O calibration line obtained for the series of standards (see Methods, Supplementary table 4a, 4b) to calculate H_2O contents of the samples; **b** and **c** – the correlation lines between IMF and H_2O and Al_2O_3 contents, multivariant correlation between IMF and both H_2O and Al_2O_3 contents (*p-value* <0.002, R^2 ~0.75, equation 2, METHODS) was used to correct the matrix effect of the analyzed materials. R- correlation coefficient.
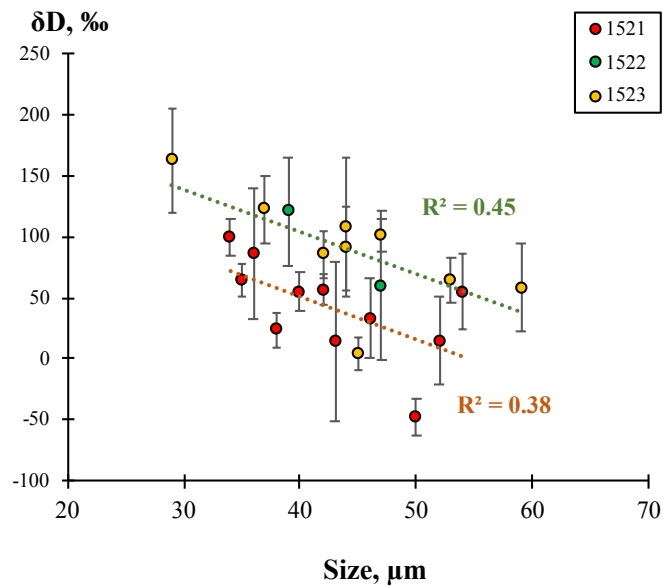
Extended Data Figure 4 |Significant correlation between isotope composition of H and size of melt inclusion in olivine of Weltevreden komatiites. Inclusion 1521-ol12 was excluded as a size outlier (120 μm).

Extended Data Figure 5 |Reconstruction of initial H_2O contents in melt inclusions. **a-** Al_2O_3 versus MgO of melt inclusions in olivine of Weltevreden komatiites. Alumina contents apparently follow olivine crystallization path of the initial komatiite melt calculated for 1521 sample[47]. **b-** Uncorrected (open circles) and corrected (filled circles) initial H_2O contents of melt inclusions. Corrected initial H_2O contents of melt inclusions follow olivine crystallization trajectory within each sample. All error bars reported as 1 S.E.